Observation analysis of land-atmosphere interactions over the Loess Plateau of northwest China

Guoyin Wang,[1] Jianping Huang,[1] Weidong Guo,[2,3] Jinqing Zuo,[1] Jiemin Wang,[4] Jianrong Bi,[1] Zhongwei Huang,[1] and Jinsen Shi[1]

Received 12 October 2009; revised 11 March 2010; accepted 21 April 2010; published 26 August 2010.

[1] Arid and semi-arid areas of the Loess Plateau over northwestern China are one of the dust aerosol source regions featured by its unique underlying surface. These areas, suffering the severe aridity trend in past decades, are also known as the transitional zone of climate and ecosystem change. To better understand the basic characteristics of the land surface energy budget, seasonal and diurnal variations of moisture and heat flux over this region, field observations collected at the Semi-Arid Climate and Environment Observatory of Lanzhou University (SACOL, 35°57′N, 104°08′E, Elev. 1965.8 m) from January 2007 to December 2008 were analyzed systematically, especially focusing on land surface energy partitioning and energy balance. The results indicate that all four radiative components had distinct seasonal and diurnal cycles, except for the diurnal variation of downward longwave radiation. They maintained high values during the growing season and low values during the non-growing season. The highest daily mean value of DSR (downward shortwave radiation, 369.2 Wm^{-2}), DLR (downward longwave radiation, 386.8 Wm^{-2}) and ULR (upward longwave radiation, 484.2 Wm^{-2}) measured in summer while the highest daily mean value of USR (upward shortwave radiation, 150.1 Wm^{-2}) occurred in winter as the snow cover. The highest surface albedo was also found in winter as a result of the snow cover. Surface albedo was lower in the growing season (wet season) due to the larger vegetation fraction and wetter soil. The components of the land surface energy budget varied seasonally except for the surface soil heat flux, and all showed strong diurnal cycles. Net radiation increased from winter to summer and decreased from summer to winter associated with the variation of DSR. Sensible (latent) heat flux was the main consumer of the available energy in winter and spring (summer and autumn). The energy imbalance problem was also identified. When the soil heat storage in the surface soil and vegetation canopy was neglected, the energy imbalance ratio was about 22%. While given the surface heat storage calculated by the thermal diffusion equation and correction method (TDEC), the imbalance ratio was only 14%. Furthermore, taking the soil heat storage into account, this ratio was only 8% in spring, and 15% in summer and autumn. Compared with the bare surface layer in spring, it is likely that a part of energy was stored in the vegetation canopy in summer and autumn. In addition, the sensible and latent heat fluxes over different land surface types of the Loess Plateau are analyzed. Sensible and latent heat fluxes are utterly different substantially over those different underlying surfaces due to the factors such as vegetation, precipitation, and soil moisture.

Citation: Wang, G., J. Huang, W. Guo, J. Zuo, J. Wang, J. Bi, Z. Huang, and J. Shi (2010), Observation analysis of land-atmosphere interactions over the Loess Plateau of northwest China, *J. Geophys. Res.*, *115*, D00K17, doi:10.1029/2009JD013372.

[1]Key Laboratory for Semi-Arid Climate Change of the Ministry of Education, College of Atmospheric Sciences, Lanzhou University, Lanzhou, China.
[2]ICGCR, School of Atmospheric Sciences, Nanjing University, Nanjing, China.
[3]Key Laboratory of Regional Climate-Environment Research for Temperate East Asia, Institute of Atmospheric Physics, Chinese Academy of Sciences, Beijing, China.
[4]Cold and Arid Regions Environmental and Engineering Research Institute, Chinese Academy of Sciences, Lanzhou, China.

0148-0227/10/2009JD013372

1. Introduction

[2] Land surface processes, which control the exchanges of energy and mass fluxes between the surface and the atmosphere, is one of the most basic aspects of climate change research. State variables that describe climate, such as air temperature, humidity, precipitation, and net radiation, are influenced by the rates at which solar energy, water vapor, and heat fluxes are exchanged between land and atmosphere [*Baldocchi et al.*, 1997]. Surface fluxes of momentum, heat,

and moisture determine to a large extent the steady state of the atmosphere [*Beljaars and Holtslag*, 1991]. Climate simulations are especially sensitive to the seasonal and diurnal variations in surface partitioning of available energy into sensible and latent heat fluxes [*Rowntree*, 1991; *Dickinson et al.*, 1991]. Improving these land-surface parameters in atmospheric numerical models is one of two key ways to enhance their prediction abilities [*Dickinson*, 1995]. In order to evaluate the long-term energy balance and evapotranspiration, numerous experimental studies have been carried at various terrestrial land-cover types (e.g., forests, grasslands, and paddy fields) throughout the world over the past decades [e.g., *Baldocchi et al.*, 1997; *Rosset et al.*, 1997; *Toda et al.*, 2002]. Recent studies have not only focused on quantifying the seasonal variations in surface exchange, but have also explored the spatial and temporal variations in sensible heat flux (H), latent heat flux (L_E), and net ecosystem CO_2 exchange (NEE) over different land surfaces in variety of ecosystems [*Yi et al.*, 2000; *Fischer et al.*, 2007; *Wohlfahrt et al.*, 2008; *Górska et al.*, 2008; *Liu et al.*, 2009]. Studies of long-term energy balance and evapotranspiration have also reported on measurements of the seasonal and diurnal variations of heat and water vapor exchanges over the tropical monsoon region of southern China and the typical steppe prairie of Inner Mongolia [e.g., *Bi et al.*, 2007; *Gao et al.*, 2009; *Li et al.*, 2009]. Although, Some field experiments have recently been carried out over the arid and semi-arid regions of China over the past 30 years, e.g., the Heihe river basin Field Experiment (HEIFE) [*Hu*, 1994; *Hu and Gao*, 1994; *Wang and Mitsuta*, 1991, 1992], the Inner Mongolia Semi-Arid Grassland Soil-Vegetation-Atmosphere Interaction (IMGRASS) [*Lu et al.*, 2002, 2005], the Field Experiment on Interaction between Land and Atmosphere in Arid Region of Northwest China (NWC-ALIEX) [*Zhang et al.*, 2005; *Bao and Lu*, 2006], the Dunhuang experiment [*Zhang et al.*, 2002], and surface layer turbulent flux observations over Naiman [*Zhang et al.*, 2001] and Tongyu [*Liu et al.*, 2004], etc. Most of those experiments have been conducted in summer, and little attention has been paid to long-term observations, especially over the arid and semi-arid areas of Loess Plateau of northwest China.

[3] Loess Plateau is the largest arid and semi-arid zone in China. Chinese loess, a widespread wind-blown deposit in northern China, covers an area of about 500,000 km^2 with a thickness of 150~300 m [*Liu*, 1985; *An*, 2000]. As the uniqueness characteristics of the loess, the monsoon, aridity history and inland deserts in central Asia can be well recorded by the loess deposits in China [*An et al.*, 2001; *Guo et al.*, 2002]. Furthermore, the special land surface physical processes of this region not only influence the regional climate and the atmospheric circulation, but also affect the monsoon circulation in China. It is an important source regions of the dust aerosol featured by its unique underlying surface, and these areas are also known as the transitional zone of climate and ecosystem change suffering the severe aridity trend in past decades [*Fu and Wen*, 2002; *Fu and Penning De Vries*, 2006]. At the same time, the Loess Plateau, having vulnerable ecological environments, is experiencing high rates of soil erosion. The Loess Plateau is rich in light and heat, both of which are beneficial to plant growth, but high potential evaporation means that water is rapidly lost from the soil profile. Water shortages and low soil moisture are the main restricting factors for the growth of vegetation and ecological systems [*Zhang and Shangguan*, 2002]. Soil moisture is entirely reliant on received precipitation. As annual rainfall is relatively low over this region and the uneven distribution in both space and time, the characteristics of soil moisture is difficult to conserve environmentally in the Loess Plateau [*Guan et al.*, 2009]. As the uniqueness of the soil, geography, and climate regimes of the Loess Plateau, it is very important and necessary to study the long-term land surface processes over this region

[4] However, abundant information about various aspects of the climate characteristics over the Loess Plateau has been obtained; little attention has been paid to long-term observations over these areas. To fill this gap, the Semi-Arid Climate and Environment Observatory of Lanzhou University (SACOL) established in 2005, provides long-term and continuous observations over the semi-arid region of the Loess Plateau in northwest China. It consists of a large set of instruments and focuses on: (1) monitoring of long-term tendencies in semi-arid climate changes; (2) monitoring of the aerosol effect on the water cycle; (3) studies of interaction between land surface and the atmosphere; (4) improving the land surface and climate models; and (5) validation of spaceborne observations [*Huang et al.*, 2008].

[5] In this study, series of 2-year continuous observations (form 1 January 2007 to 31 December 2008) were used to investigate the seasonal variation of climate variables and energy flux over semi-arid regions of northwest China. This study is objective to improve our understanding of energy partitioning, energy balance, and water cycle over the land surface.

2. Observational Experiments and Method of Data Analyses

2.1. Site Description and Data Collection

[6] SACOL, located approximately 48 km away from the downtown of Lanzhou city on the southern bank of the Yellow River in Gansu province northwest China (35°57′N, 104°08′E, 1965.8 m above sea level), is one of the reference sites of the international Coordinated Energy and Water Cycle Observations Project (CEOP). The parent soil material is mainly the Quaternary aeolian loess with the main soil type of sierozem. The surface is mainly covered by short grass with species of Stipa bungeana, Artemisia frigida, and Leymus secalinu which is usually less than 15 cm tall and covered less than 80% of the surface in summer and autumn (Figure 1a). The site is located on a nearly north-south mesa with a fetch length of about 120 m in the most common wind direction. The mesa has a limited width of about 200 m from the east to the west, and is about 600 m in length from the north to the south. There is a large V shape valley to the west of the site and a small one to the east. SACOL was established at the typical semi-arid region of Yuzhong campus of Lanzhou University in 2005 and started continuous observation in May 2006. The observatory includes an array of instrumentation that measures (1) boundary layer meteorological parameters, (2) surface radiation, (3) surface flux, (4) soil heat and water moisture, (5) ambient air quality, (6) aerosol optical properties, (7) temperature and water vapor profiles, and (8) sky conditions. All the data used in this paper

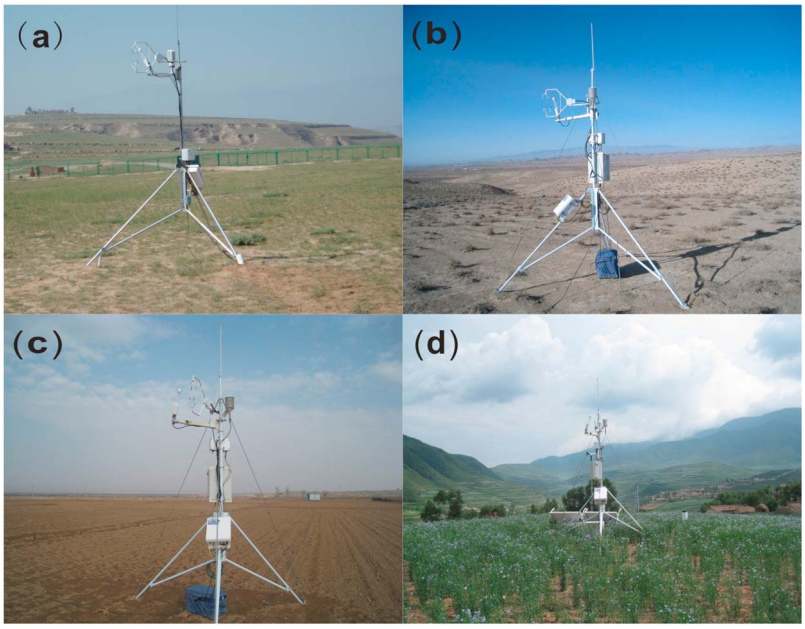

Figure 1. Field sites with the eddy covariance systems at (a) SACOL, (b) the Jingtai hill site (JH), (c) the Jingtai farmland site (JF), and (d) the Xinglong Mountain site (XM).

were averaged over 30-min intervals, except for the raw eddy covariance.

[7] Following the establishment of SACOL, the first Sino-American dust storms observation was made in March, 2008. Measurements were composed by three observatories: SACOL, the Jingtai mobile observatory, and the Zhangye mobile observatory. The Jingtai mobile observatory was set up in a semi-arid area (37°20′N, 104°08′E) and approximately 300 km to the north of SACOL. A pair of experiments was carried out at this region, which were located at the Jingtai hill (referred to as JH, 1617m above sea level; Figure 1b) and the Jingtai farmland (referred to as JF, 1592m above sea level; Figure 1c), respectively. And the distance between these two sites was about 1 km away. The underlying surface of JH during the experiment was covered by Stipa bungeana, Artemisia frigida, and JF was a maize field irrigated with water from the Yellow River. Flux data had been collected in JH from 21 to 31 March, and JF from 17 April to 30 May, 2008 respectively.

[8] SACOL was situated at the semi-arid area of China-Loess Plateau. It is meaningful that the Xinglong Mountain, an isolated oasis surrounding by the semi-arid area, is approximately 25 km away from SACOL. In order to understand the differences of the meteorological elements between these two surface types, a temporal experiment site was set up at Xinglong Mountain (referred to as XM, 35°46′N,104°03′E, 2481m above sea level) in June 2008. It is similar with SACOL that the XM experiment field was located in a transitional zone between humid monsoon and dry non-monsoon climate zones, however, the vegetation coverage at XM was extraordinarily large. Flux data had been collected from 1 July to 30 September, 2008 (Figure 1d), and the underlying surface was benne at XM during these experiment time.

[9] All the information about the above four sites are listed in Table 1.

2.2. Micrometeorological Measurements

[10] The main instruments at SACOL from which we collected data for our study include a surface layer meteorological tower, a radiation flux observation system, the eddy covariance system (EC) to measure the turbulent fluxes, and a soil temperature/humidity measuring system. XM used the same model as SACOL, while Jingtai just used the eddy covariance systems.

[11] Boundary layer meteorological measurements include wind speed (014A-L, Met One), air temperature and relative humidity (HMP45C-L, Vaisala) at 1, 2, 4, 8, 12, 16 and 32 m,

Table 1. Site Information at SACOL, Jingtai Hill, Jingtai Farmland and Xinglong Mountain During the Measurement Periods[a]

	Site			
	SACOL	JH	JF	XM
Location	35°57′N, 104°08′E	37°20′N, 104°08′E	37°20′N, 104°08′E	35°46′N, 104 °03′E
Elevation	1965.8 m	1617 m	1592 m	2481 m
Dominant species	Stipa bungeana, Artemisia frigida, and Leymus secalinu	Stipa bungeana, Artemisia frigida	maize	benne
Canopy height	10 cm	5 cm	15 cm	30 cm
Measurement period	January 2007– December 2008	21–31 March, 2008	17 April to 30 May, 2008	1 July to 30 September, 2008

[a]Jingtai hill, JH; Jingtai farmland, JF; Xinglong mountain, XM.

Table 2. Measurement Instruments and Quantities Measured at SACOL

Parameter/Variable Name Description	Range	Measurement Height	Instrument
Wind speed sensor	0–45 m/s	2.0 m	Met One, 014A-L
Humidity probe	0–100%	2.0 m	Vaisala, HMP45C-L
Temperature probe	−45–60°C	2.0 m	Vaisala, HMP45C-L
Barometric pressure sensor	600–1060 millibar	8.0 m	Vaisala, CS105
Tipping bucket rain gage	0–15 mm	0.3 m	TE525MM-L, R.M Young
Pyranometer (SW flux)	0–1200 W m^{-2}	1.5 m	Kipp & Zonen, CM21
Pyrgeometer (LW flux)	0–700 W m^{-2}	1.5 m	Kipp & Zonen, CG4
3-D Sonic anemometer		3.0 m	Campbell, CSAT-3
Opened path infrared CO_2 and H_2O analyzer		3.0 m	Li-Cor, LI7500
Water content reflectometer	0–70 VV^{-1}	5, 10, 20, 40, 80 cm	CAMPELL, CS616L
Soil temperature profile	−50–70°C	2, 5, 10, 20, 50, 80 cm	Hukseflux, STP01-L
Soil heat flux plate	−300–300 W m^{-2}	5, 10 cm	Hukseflux, HFP01SC-L

and wind direction (034B-L, Met One) at 8 m, with signals logged to a data logger (CR23X, Campbell) and recorded at half-hour intervals. The measurement of skin temperature is made with a Precision Infrared Thermo-couple Sensor (IRTS-P, Apogee). Barometric pressure is measured using a CS105 Barometric Pressure Sensor (Vaisala) over a 600 to 1060 hPa range. Precipitation is measured with a tipping bucket Rain Gage (TE525MM-L, Texas Electronics) at 0.1 mm increments.

[12] The surface radiation monitoring system consists of upward and downward pyranometers (CM21, Kipp & Zonen) for outgoing and incoming short-wave radiation; and upward and downward pyrgeometers (CG4, Kipp & Zonen) for outgoing and incoming longwave radiation.

[13] The fluxes of momentum, latent and sensible heat are measured at 3.0 m with a three-axis Sonic Anemometer (CSAT3, Campbell) pointed toward the prevailing wind direction, and an opened path infrared CO_2 and H_2O analyzer (LI7500,LI-COR) (Figure 1). These signals are logged to a data logger (CR5000, Campbell) at 10 Hz. The sensors for measuring CO_2 and H_2O turbulence (LI7500) are calibrated in May every year. All of the necessary procedures for corrections and quality control of the turbulent fluxes are applied during post-field data processing, such as coordinate rotation by the planar fits method (PF) [*Wilczak et al.*, 2001], frequency response corrections [*Moore*, 1986; *Massman*, 2000, 2001], sonic temperature correction [*Schotanus et al.*, 1983], WPL correction [*Webb et al.*, 1980], and quality control after *Foken et al.* [2004].

[14] To complete the surface energy balance, soil heat fluxes (HFP01SC-L, Hukseflux) are measured at 5 and 10 cm depth. Soil moisture is measured with a water content reflectometer (CS616-L, Campbell) at 5, 10, 20, 40 and 80 cm depths; and soil temperature with a soil temperature profile (STP01-L, Hukseflux) sensor at 2, 5, 10, 20, 50 and 80 cm depths. For more details see *Huang et al.* [2008].

[15] The measurement parameters used in this study are listed in Table 2. A linear interpolation scheme was used to fill in missing data and to construct a regularly spaced data.

[16] In addition, fluxes of momentum, latent and sensible heat are measured at 3.0 m at JH, 2.85 m at JF, and 2.82 m at XM, respectively, with a three-axis Sonic Anemometer (CSAT3, Campbell) pointed into the prevailing wind direction, and an opened path infrared CO_2 and H_2O analyzer (LI7500,LI-COR) (Figure 1). These signals are logged to a data logger (CR1000, Campbell) at 10 Hz.

2.3. Method of Data Analyses

2.3.1. Surface Albedo

[17] The land surface albedo is calculated by the formula below:

$$\alpha = S_u/S_d, \tag{1}$$

where S_u is the total upward solar radiation (the surface reflected solar radiation flux) and S_d is the total downward solar radiation reaching the land surface. Surface albedo is calculated based on the S_u and S_d measured by pyranometer CM21 every half hourly. To avoid the influence of solar elevation angle on the surface albedo, daily average surface albedo is obtained from half hourly average albedo when the solar elevation angle is lager than 30°.

2.3.2. Surface Energy Balance Analyses

[18] At the surface, the net radiative energy should be balanced by the surface soil heat flux (G_0), sensible heat flux (H), and latent heat flux (L_E). The surface energy balance over the semi-arid grass land can be expressed as

$$R_n = H + L_E + G_0 + R_e, \tag{2}$$

where R_n is the net radiation, H and L_E are respective the sensible and latent heat fluxes, G_0 is the surface soil heat flux, and R_e is the residual energy involved in various processes, such as photosynthesis and respiration [*Harazono et al.*, 1998; *Burba et al.*, 1999].

[19] We determine R_e from the formula: $R_e = R_n - (H + L_E + G_0)$. R_n was calculated by using four radiation components. Eddy fluxes of sensible heat flux and latent heat flux were calculated as

$$H = \overline{\rho} c_p \overline{w'T'}, \tag{3}$$

$$L_E = \overline{\rho} L_v \overline{w'q'}, \tag{4}$$

where ρ, C_p and L_v are the density of air (kg m^{-3}), the specific heat of air (J kg^{-1} K^{-1}), and the latent heat of vaporization (J kg^{-1}), respectively. W', T', and q' are the fluctuations in the vertical wind component (m s^{-1}), air temperature (K) and specific humidity, respectively. The data quality control have been strictly processed before acquiring the turbulent fluxes, more information about the processing of the calculation turbulent fluxes and QA/QC (quality assurance/quality control) please refer to the work by *Zuo et al.* [2009].

[20] Surface soil heat flux G_0 is estimated as follows. The one-dimensional soil Thermal Diffusion Equation (TDE) is

$$\frac{\partial \rho_s c_s T}{\partial t} = \frac{\partial G}{\partial z} \tag{5}$$

$$G = \lambda_s \frac{\partial T}{\partial z}, \tag{6}$$

where t (s) is the time, z (m) is the soil depth (positive if downward), T (K) is the soil temperature, $\rho_s c_s$ (J kg^{-1} K^{-1}) is the soil heat capacity, λ_s (W m^{-1} K^{-1}) is the soil thermal conductivity, and G (W m^{-2}) is the soil heat flux (positive if downward).

[21] Integrating equation (5) gives

$$G(z) = G(z_{\mathrm{ref}}) + \int_{z_{\mathrm{ref}}}^{z} \frac{\partial \rho_s c_s T(z)}{\partial \mathrm{t}} \mathrm{dz}, \tag{7}$$

where $G(z_{ref})$ is the soil heat flux at a reference depth (z_{ref}).

[22] Given temperature profile T (z_i), the discretized form of equation (7) is

$$G(z,t) = G(z_{\mathrm{ref}},t) + \frac{1}{\Delta t}\sum_{z_{\mathrm{ref}}}^{z}[\rho_s c_s(z_i, t+\Delta t)T(z_i, t+\Delta t) - \rho_s c_s(z_i,t)T(z_i,t)]\Delta z. \tag{8}$$

[23] The heat capacity can be calculated from soil water content and soil porosity that can be easily measured. Therefore, the key issue to calculate soil heat flux is how to make a reliable temperature profile from limited observations. *Yang and Wang* [2008] proposed a new method to correct the temperature profile. For the convenience of description of this method, it is named after TDEC (Thermal Diffusion Equation and Correction). In this paper, the surface soil heat flux G_0 is estimated by the TDEC method.

3. Results and Discussion

[24] To examine whether our measurements (SACOL) were representative for the climate of the study area, corresponding historical data obtained from a meteorological station from January 1956 to December 2008 were plotted (Figure 2). The meteorological station was located in Yuzhong (35°52′N, 104°09′E) at approximately 1875 m above sea level, and approximately 7 km from SACOL. The historical data have been collected at 2:00, 8:00, 14:00, and 20:00 (local time) as routine observations. The results show that our measurements well represent the meteorological situation over the past 53 years (1956–2008), and therefore can be considered representative of the climate of this region. Figures 2a–2d show the daily means of wind speed (*Ws*), air temperature (T_{air}), water vapor pressure (e) and air pressure (P), and Figure 2e presents the daily total precipitation (*Prec.*), for both SACOL and historical data.

[25] As shown in Figure 2, the annual wind speed at SACOL (2.7 m/s) was slightly greater than the 53-yr-average annual mean wind speed (1.7 m/s). The maximum value of daily mean wind speed was 9.3 m/s in February 2007.

[26] Air temperature had a large seasonal variation. At SACOL, daily mean air temperature reached a maximum (297.1 K) in August 2007, while the lowest air temperature (255.6 K) was recorded in January 2008. The difference between the highest air temperature and lowest air temperature was 21.5 K from January 2007 to December 2008, and the annual mean air temperature was 281.5 K. In historical data form January 1956 to December 2008, the annual mean air temperature was 280.0 K. Although SACOL is 90 m higher in elevation than the Yuzhong meteorological station, the annual mean air temperature at SACOL was larger than the 53-yr-average annual mean air temperature by ~1.5 K. This biases can be explained by the unlike environment of locations, inconsistent types of instrumentations and discrepancy of measurement heights between these two sites. Furthermore, the fact that SACOL have the similar trend of the variation with Yuzhong meteorological station demonstrates that SACOL can well representative for the climate of the study area.

[27] Water vapor pressure also showed significant seasonal variation. The 53-yr-average annual mean water vapor pressure was 7.2 hPa, and the average for SACOL was only 6.8 hPa. Air pressure varied seasonally as well, but was in reverse phase to air temperature and water vapor pressure. The 53-yr-average annual mean air pressure at Yuzhong meteorological station and SACOL were 811.5 hPa and 802.8 hPa, respectively. The difference between the historical and SACOL data is mainly due to the higher elevation (+90 m) of SACOL.

[28] The 53-yr-average of annual precipitation (*Prec.*) at the Yuzhong meteorology station was 370.2 mm. Precipitation was unevenly distributed throughout the year, with more than 90 percent of annual precipitation falling between May and October (wet season). Annual precipitation at SACOL was 559.0 mm in 2007 and 335.8 mm in 2008. Clearly, 2007 was a wetter year (50% above the climate-average annual precipitation) and 2008 was a drier year (receiving 90% of the climate-average annual precipitation). Therefore, during the study period, the variability of interannual precipitation was quite large.

3.1. Seasonal and Diurnal Variation

3.1.1. Variation in Radiation Components

[29] Figure 3 shows the seasonal and interannual variations of the four radiation components at SACOL: (1) downward shortwave radiation (hereafter, DSR), (2) upward shortwave radiation (USR), (3) downward longwave radiation (DLR), and (4) upward longwave radiation (ULR), and the daily average surface albedo is presented in Figure 3e. To eliminate the effects of diurnal variation, a 7-day moving average was calculated for these four components.

[30] As evident from Figure 3, all the four radiative components varied seasonally and dramatically, consistent with the variations of air temperature, water vapor pressure, air pressure, and precipitation in Figure 2. ULR and DSR had the strongest seasonal and interannual variability, especially during summer. Both DSR and USR were strongly affected by clouds and aerosols, and maintained high values during the wet season. The highest daily mean value of DSR was 369.2 Wm^{-2}, measured in June 2008. While the highest daily mean value of USR (150.1 Wm^{-2}) did not appear at the same time as that of DSR as expected, because of high surface albedo in winter. Seasonal variations of DLR and ULR were not strongly affected by cloud, aerosol, or snow cover, and

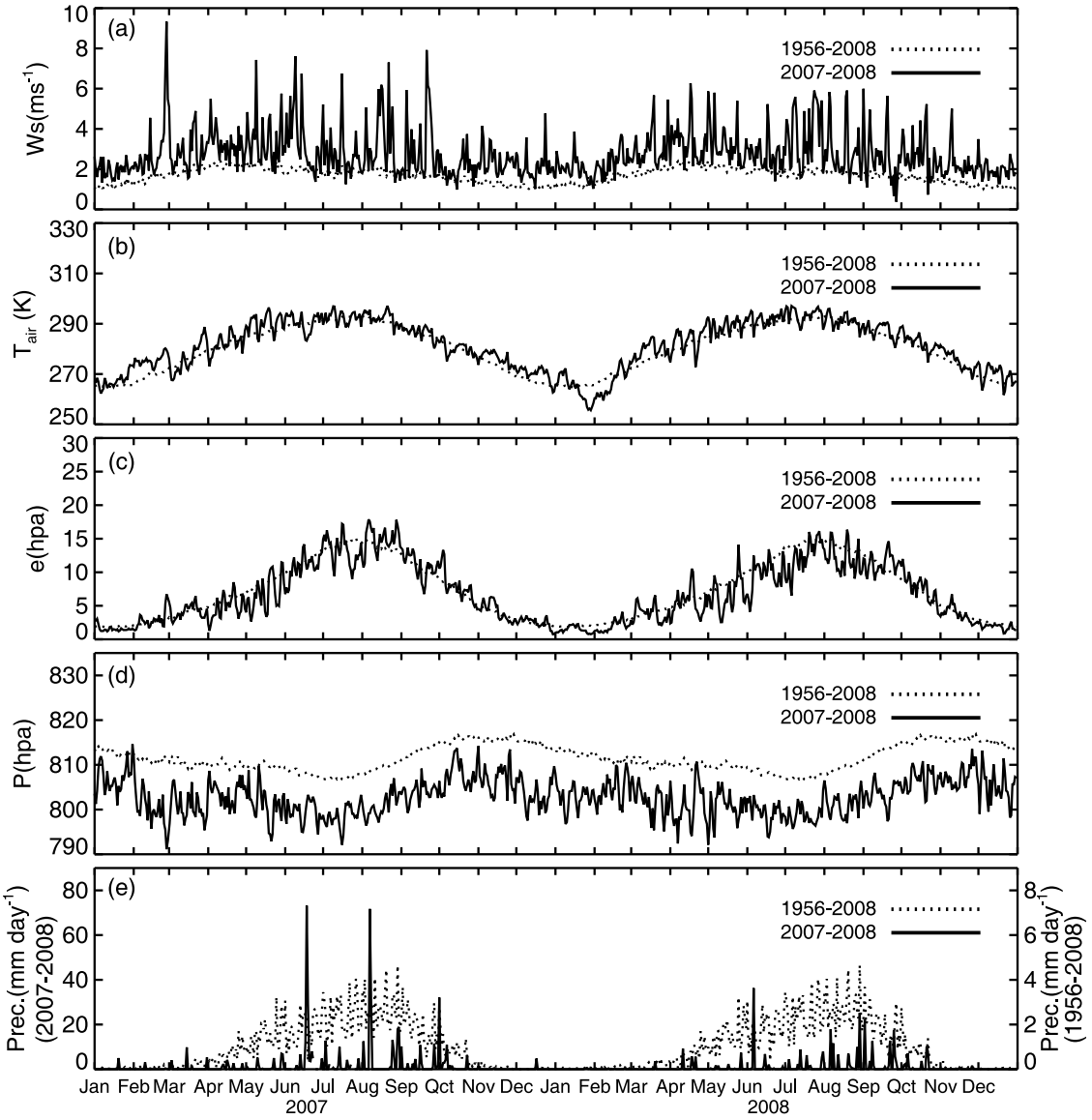

Figure 2. (a) Wind speed (*Ws*), (b) air temperature (T_{air}), (c) water vapor pressure (*e*), (d) air pressure (*P*), and (e) precipitation (*Prec.*) measured at SACOL from January 2007 to December 2008 (solid line) compared to the climate data collected at Yuzhong meteorological station from January 1956 to December 2008 (dotted line).

both of them maintained high values during the growing season. The maximum of daily mean values of DLR and ULR were 386.8 Wm^{-2} and 484.2 Wm^{-2} occurring in August 2007 and July 2008, respectively. The lowest values of DLR (162.6 Wm^{-2}) and ULR (220.9 Wm^{-2}) occurred in January 2008. All four radiative components exhibited significant differences between 2007 and 2008 due to the different weather conditions and underlying surface conditions, as shown in Figures 3a–3d.

[31] Surface albedo is one of the most important properties of the underlying surface. It determines the surface energy balance and greatly influences the energy and water cycles of the ecosystems by influencing the vegetative evapotranspiration, photosynthesis, and biochemical processes [*Bao and Lu*, 2006]. The seasonal variation of daily averaged surface albedo is shown in Figure 3e. The highest surface albedo value (0.9) occurred in winter, which is caused by snow cover. The value of mean surface albedo value not influenced by snow cover was 0.187 ± 0.023 from January 2007 to December 2008. This value is lower than those values observed in HEIFE Gobi (0.228) and desert (0.246) [*Zhou et al.*, 1992], the Dunhuang Gobi (0.255 ± 0.023) [*Zhang et al.*, 2002], and the typical steppe prairie in Inner Mongolia (0.22) [*Gao et al.*, 2009], but it is higher than the value observed over grassland in the tropical monsoon region of southern China (0.11 to 0.13) [*Bi et al.*, 2007].

[32] Surface albedo is strongly influenced by solar elevation angle and surface conditions, such as soil moisture, vegetation cover, roughness, and so on. Excluding the influence of solar elevation angle, the soil moisture is the key parameter in controlling the variation of surface albedo. Surface albedo decreases with increasing soil moisture

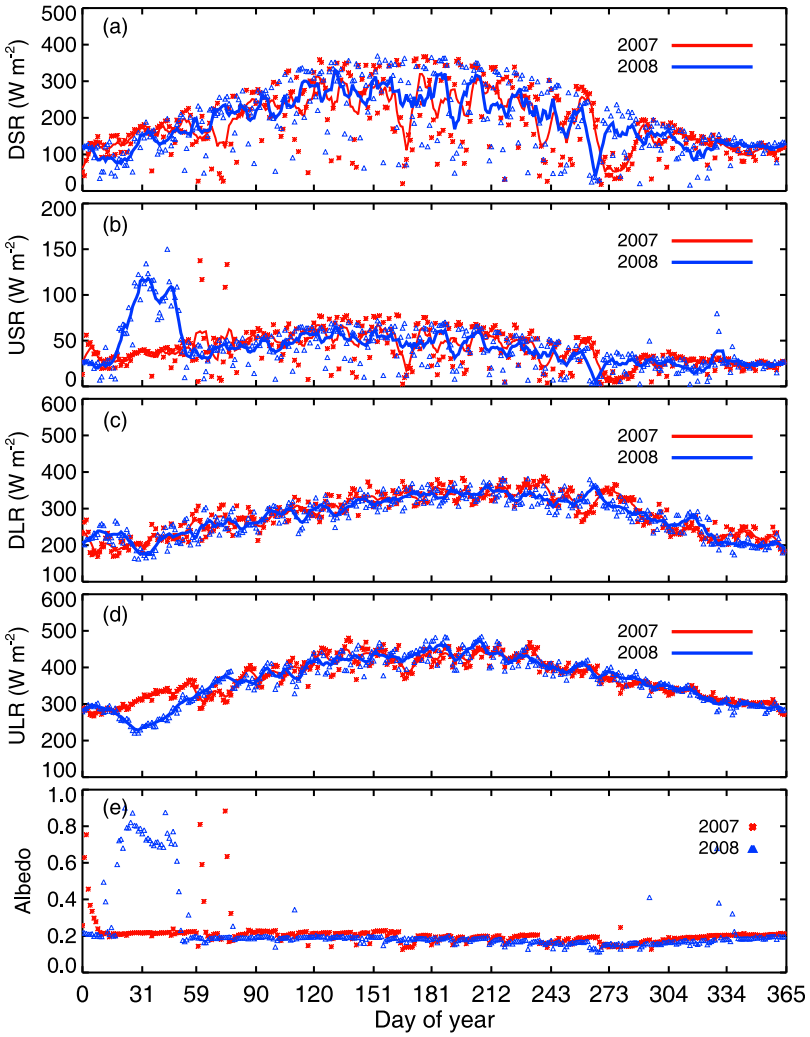

Figure 3. Variations of the daily mean (a) downward shortwave radiation (DSR), (b) upward shortwave radiation (USR), (c) downward longwave radiation (DLR), (d) upward longwave radiation (ULR), and (e) surface albedo; the solid line represents the moving average smoothed by 7 days at SACOL from January 2007 to December 2008.

content [*Wang et al.*, 2005]. *Guan et al.* [2009] also indicate that surface albedo decreases when soil moisture content increases with a typical exponential relationship at SACOL. Seasonal variation of surface albedo in 2008 was similar to that in 2007, maintaining high values in winter and spring, and decreasing from May to October (wet season) when soil moisture (Figures 9c and 9d) and the vegetation fraction was at its highest. However, surface albedo is larger in 2007 (0.195 ± 0.024) than that in 2008 (0.179 ± 0.019) while precipitation in 2007 is 223.2 mm larger than that in 2008. This can be explained that the higher total precipitation in 2007 primarily comes from the two strong precipitation events, which supply chance to recharge deep soil moisture (e.g., 80cm depth), and the surface dries out after precipitation event. More weak precipitation events in 2008 supply more chances to recharge surface soil moisture at depths of 5 cm to 20 cm (Figures 9c and 9d). Therefore, surface moisture in 2008 is generally higher than 2007, and surface albedo is larger in 2007 than that in 2008. Both of soil moisture and surface albedo show large interannual variations.

[33] To investigate the diurnal variation of the radiation components, we used a composite analysis method. The annual means of diurnal variation for DSR, USR, DLR, and ULR from January 2007 to December 2008 are shown in Figure 4, and the short lines are error bars. Diurnal variation for all four radiation components was significant except for DLR. The distributions of DSR and USR are symmetrical with a maximum 608.4 Wm^{-2} and 129.1 Wm^{-2}, respectively, at 13:30 local time. ULR had a similar pattern to DSR and followed the expected warming and cooling of the surface. The large variability of DSR and USR was likely associated with variations in clouds and aerosols.

3.1.2. Variations of Energy Components

[34] Figure 5 shows the seasonal and interannual variations of daily mean (1) net radiation (R_n), (2) sensible heat flux (H), (3) latent heat flux (L_E), and (4) surface soil heat flux ($G_{TDEC,0}$) estimated by the TDEC method. The four radiation components (i.e., DSR, USR, DLR, and ULR) used to calculate R_n, and H and L_E were measured by fast response instruments and calculated using equations (3) and (4). To eliminate the

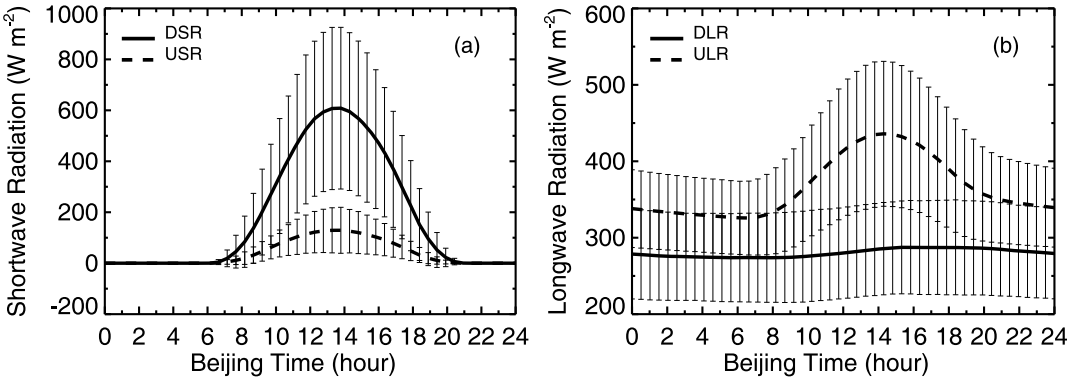

Figure 4. Diurnal cycle and standard deviation of (a) downward shortwave radiation (DSR) and upward shortwave radiation (USR) and (b) downward longwave radiation (DLR) and upward longwave radiation (ULR) at SACOL from January 2007 to December 2008.

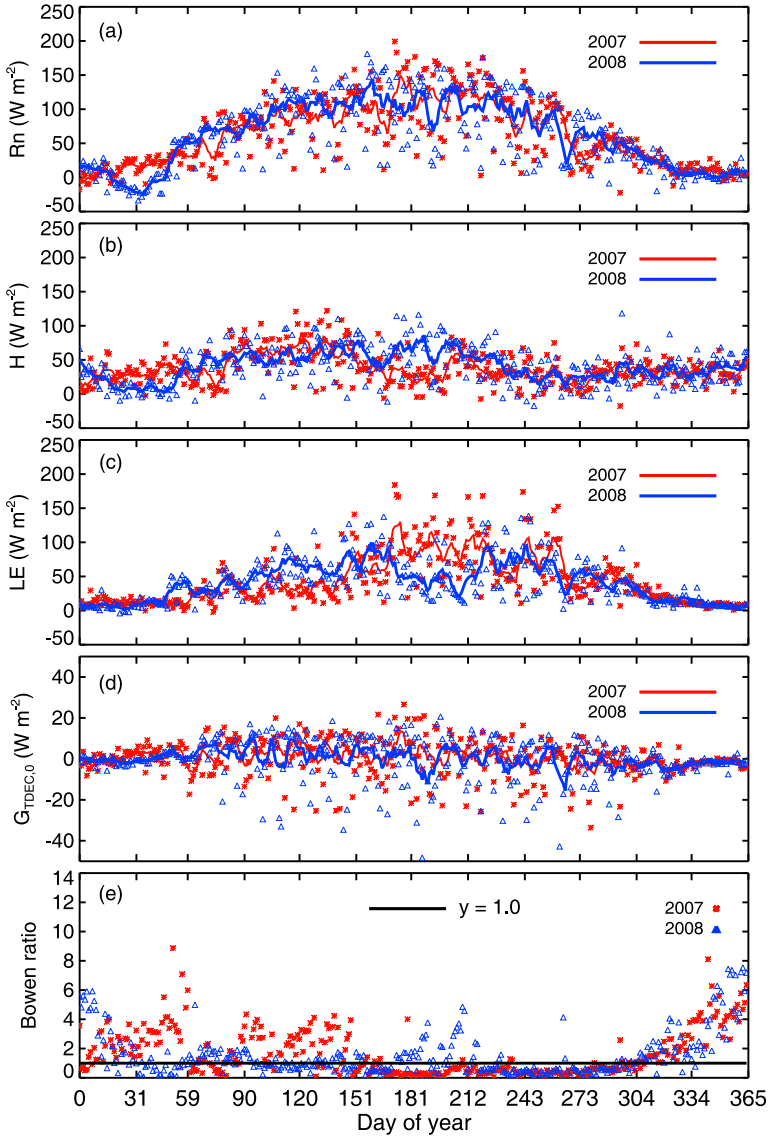

Figure 5. Variations of the daily mean (a) net radiation (R_n), (b) sensible heat flux (H), (c) latent heat flux (L_E), (d) surface soil heat flux ($G_{TDEC,\ 0}$), and (e) Bowen ratio; the solid line depicts the moving average smoothed by 7 days at SACOL from January 2007 to December 2008.

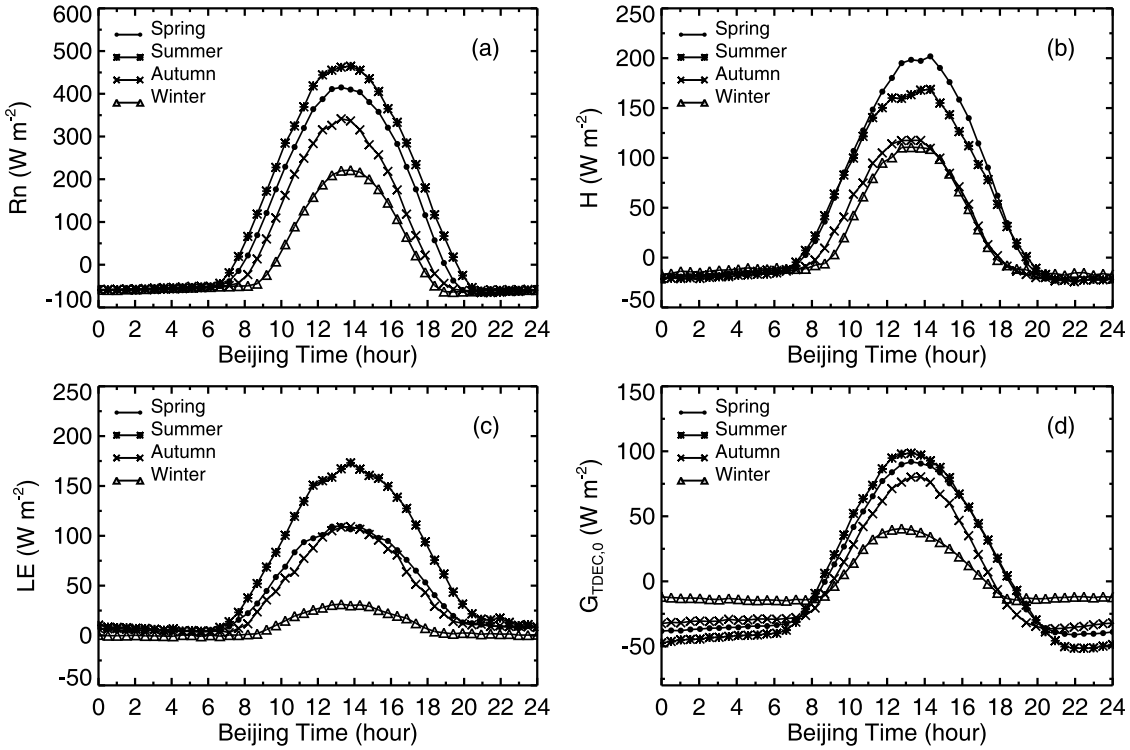

Figure 6. Diurnal cycle of the seasonal mean (a) net radiation (R_n), (b) sensible heat flux (H), (c) latent heat flux (L_E), and (d) surface soil heat flux ($G_{TDEC,\ 0}$) at SACOL from January 2007 to December 2008.

effects of diurnal variation, a 7-day moving average was calculated for the four energy components. The R_n, H, and L_E showed considerable seasonal variation, except the surface soil heat flux $G_{TDEC,0}$. R_n had a similar pattern to DSR, which had the largest seasonal and interannual variability, especially during summer. H was the main consumer of R_n during the dry season, whereas L_E was the main consumer of R_n during the wet season. There was no obvious change in $G_{TDEC,0}$.

[35] Figure 5e shows the seasonal variation of the Bowen ratio, which is defined as the ratio of daily average H and L_E. The Bowen ratio showed considerable seasonal variation over the study period. Bowen ratio in 2007 is generally higher than that in the 0~151 days 2008. It is mainly because the drought trend extended from 2006 to the summer of 2007 and hence the higher soil moisture content appeared in 2008 during these days. As a result of higher precipitation in growing season of 2007, Bowen ratio is almost far below 1.0 and latent heat flux fraction is much larger. However, soil moisture is the key parameter not only in controlling variation of albedo, but also influencing the ratio of net radiation partitioning into latent and sensible heat fluxes. Evapotranspiration, especially transpiration from vegetation, primarily

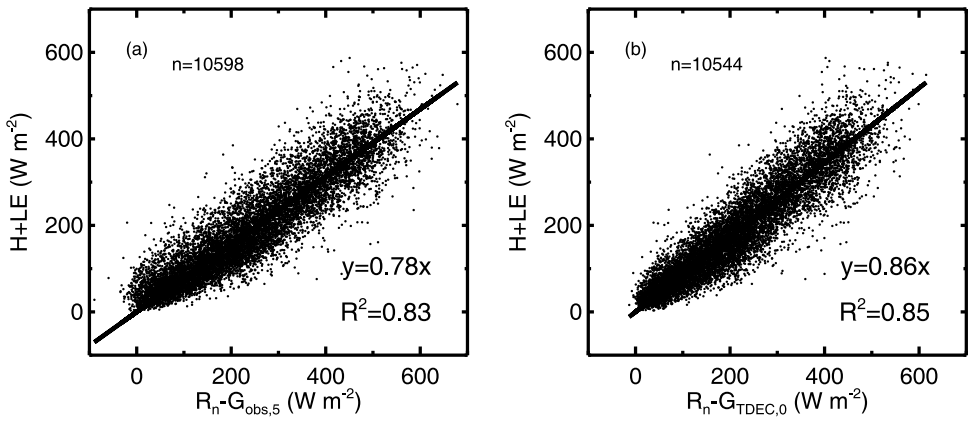

Figure 7. Intercomparison of the measured sensible and latent heat fluxes (H+L_E) against available energy (R_n–G_0) at SACOL from January 2007 to December 2008. The data represent half-hourly averages. (a) $G_{obs,5}$ is the soil heat flux observed at 5 cm depth. (b) $G_{TDEC,0}$ is the surface soil heat flux calculated from the TDEC method.

Table 3. Seasonal Energy Balance Conditions[a]

	Spring	Summer	Autumn	Winter
$(H+ L_E)/(R_n-G_{obs,5})$	0.83	0.78	0.75	0.67
$(H+L_E)/(R_n-G_{TDEC,0})$	0.92	0.85	0.85	0.73

[a]Here $(H+ L_E)/(R_n-G_{obs,5})$ and $(H+ L_E)/(R_n- G_{TDEC,0})$ are calculated by sensible and latent heat fluxes $(H+L_E)$ against available energy $(R_n-G_{obs,5})$ and $(R_n-G_{TDEC,0})$, respectively. $G_{obs,5}$ is the soil heat flux plate observed at 5 cm depth; $G_{\mathrm{TDEC},0}$ is the surface soil heat flux calculated at the land surface by the TDEC method.

Table 4. Seasonal Means of the Energy Partitioning Conditions[a]

	Spring	Summer	Autumn	Winter
H/R_n	0.46	0.33	0.32	0.47
L_E/R_n	0.27	0.35	0.35	0.14
$G_{TDEC,0}/R_n$	0.21	0.20	0.22	0.18

[a]H/R_n, L_E/R_n, and $G_{TDEC,0}/R_n$ are the ratios of sensible heat flux (H), latent heat flux (L_E) and the surface soil heat flux ($G_{TDEC,0}$) to the net radiation, respectively.

depends on soil moisture at root depth. Weak precipitation events in 2008 didn't have chance to recharge soil moisture at 80 cm depth, therefore, latent heat flux in growing season 2007 is higher than that in 2008, especially during days 175~225.

[36] Figure 6 shows the seasonal mean diurnal cycles of R_n, H, L_E, and $G_{TDEC,0}$. All components exhibited distinct diurnal cycles. As illustrated in Figure 6a, the range of the diurnal cycle of R_n increased from winter to summer and decreased from summer to winter, implying that the diurnal variation of R_n was significant in summer and weak in winter. Figure 6b shows that the diurnal variation of H was largest during spring and summer and smallest during autumn and winter. As indicated by Figure 6c, L_E had an obvious diurnal variation during summer which became small during spring and autumn, and almost absent during winter. Finally, as shown in Figure 6d, $G_{TDEC,0}$ had a similar and obvious diurnal variation in spring, summer, and autumn, but became very small in winter.

3.2. Surface Energy Balance Closure

[37] All atmospheric models are based on the principle of surface energy balance, and large closure errors are unacceptable. Figure 7 shows the inter-comparison of $H+L_E$ and R_n-G_0. We were concerned with data quality and reliability as the number of flux stations has increased to study surface energy balance closure. In this work, analysis of the surface-heating rate focused on data collected during rain-free times because the sonic anemometer displayed large errors during and after rainfall events. Data collected during calibration activities, equipment modification, and large transient fluctuations were also neglected. Analyses were also limited to situations in which H and L_E were all larger than zero because the unavailable measurement errors would be significant when the energy components were close to zero. In Figure 7a, we neglected soil heat storage and used the soil heat flux observed at 5 cm ($G_{obs,5}$) by the soil heat flux plates to replace G_0. The surface heating rate, defined as the ratio of measured $(H+L_E)$ against available energy (R_n-G_0), was 0.78, and the correlation coefficient between $H+L_E$ and $R_n-G_{obs,5}$ was 0.83. In Figure 7b, we used $G_{TDEC,0}$ to replace G_0. In this case, the surface heating rate was 0.86, and the correlation coefficient between $H+L_E$ and R_n-G_0 was 0.85. Clearly, approximately 8% of energy was stored in the top 5cm soil layer, indicating that soil heat storage should not be neglected.

[38] To understand energy closure issue at SACOL, the seasonal mean ratio of the measured $(H+L_E)$ against available energy (R_n-G_0) was calculated (Table 3). Neglecting soil heat storage, the surface heating rates were calculated as 0.83, 0.78, 0.75, and 0.67 in spring, summer, autumn, and winter, respectively. However, when incorporating the soil heat storage, the surface heating rates were calculated to be 0.92, 0.85, 0.85, and 0.73 in spring, summer, autumn, and winter, respectively. That is, if the surface heat storage was considered, surface heating rates were increased by 0.09, 0.07, 0.10, and 0.06 in spring, summer, autumn, and winter, respectively. Notably, the surface heating rate was 0.92, very close to the theoretical value 1.0 in spring, but only 0.85 in summer and autumn.

[39] Theoretically, surface heating rate should be very close to 1.0, but the energy imbalance was found in our measurements. Other major field campaigns have also encountered such energy imbalances, which caused difficulties for subsequent climate applications [e.g., *Kahan et al.*, 2006]. Previous researchers [*Foken and Oncley*, 1995; *Panin et al.*, 1996; *Wicke and Bernhofer*, 1996; *Foken et al.*, 1999; *Kahan et al.*, 2006] reported that the causes of imbalance of the energy budget were usually related to the errors/uncertainties

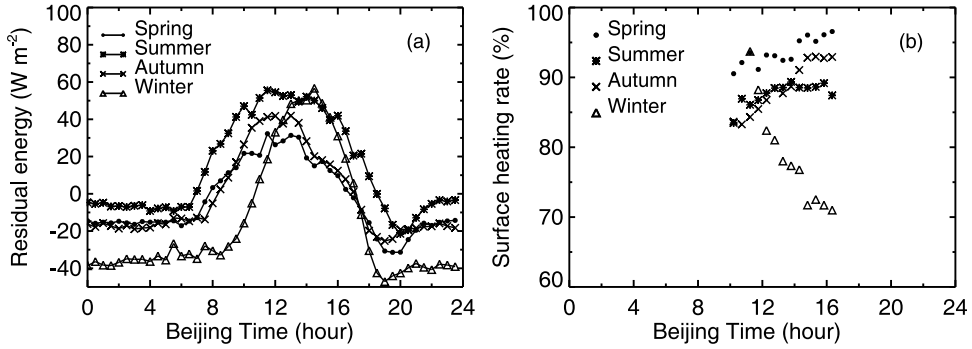

Figure 8. Diurnal cycle of (a) the residual energy ($R_e = R_n - H - L_E - G_{TDEC,0}$) and (b) the surface heating rate during daytime (10:00–16:00) for the four seasons at SACOL from January 2007 to December 2008.

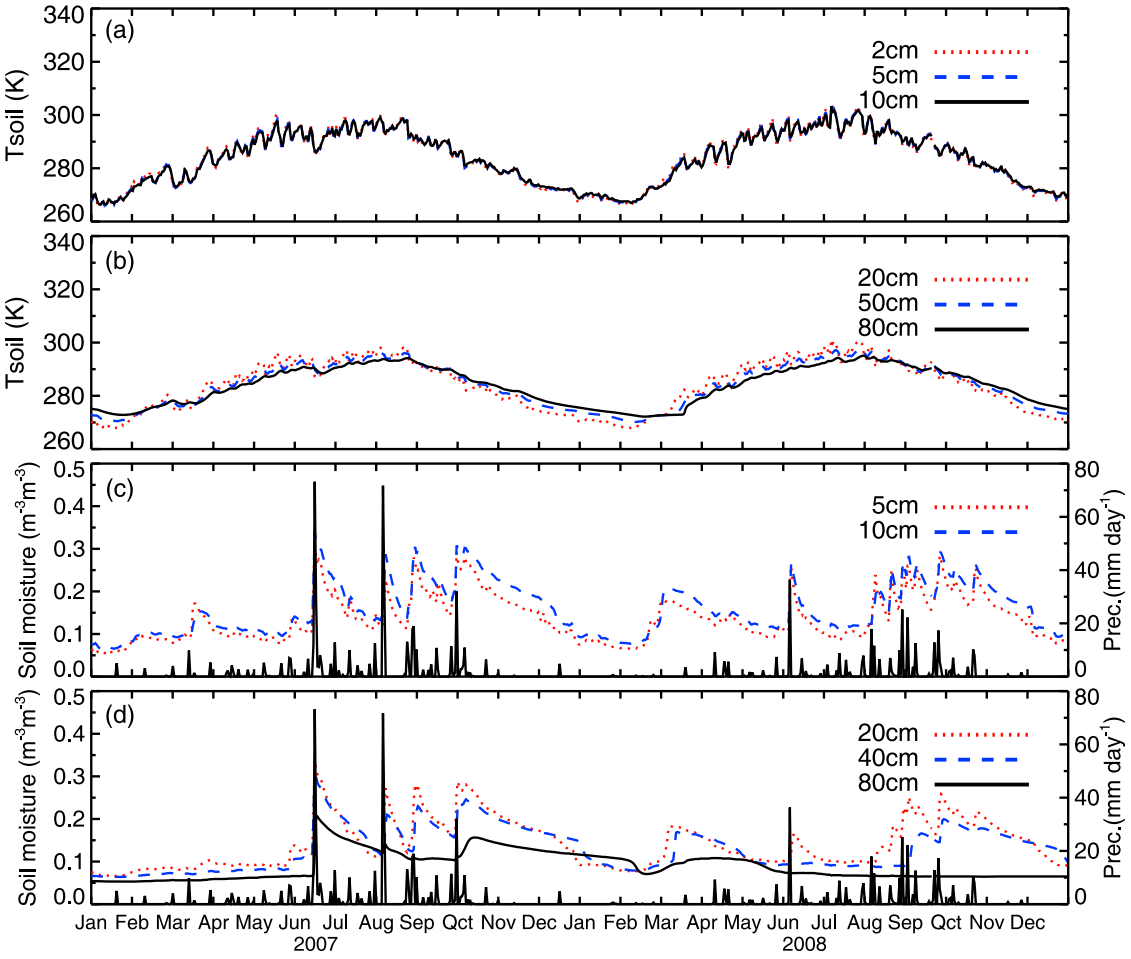

Figure 9. (a–d) Seasonal variations of daily mean soil temperature (K) at depths of 2, 5, 10, 20, 50 and 80 cm; soil moisture at depths of 5, 10, 20, 40, and 80 cm; and 24- hour precipitations at SACOL from January 2007 to December 2008.

in individual energy component measurements and the influence of different footprints on the individual energy components.

[40] The seasonal mean of diurnal variation of residual energy ($R_e = R_n - H - L_E - G_0$) and the surface heating rate during daytime (10:00–16:00) for the four seasons at SACOL from January 2007 to December 2008 are plotted in Figure 8. The diurnal variation pattern of R_e was similar to that of R_n, with both having substantial diurnal variation. R_e was smallest in spring and largest in summer and winter in Figure 8a. As illustrate in Figure 8b, the surface heating rate is lower in winter, associate with the larger R_e. The highest surface heating rate occurred in spring which is generally larger than that in summer and autumn. Considering the soil heat storage when the surface heating rate was calculated, the diurnal variation of surface heating rate during the day time was similar to the seasonal energy balance conditions (($H+ L_E$)/($R_n- G_{TDEC,0}$)) in Table 3.

3.3. Energy Partitioning at the Land Surface

[41] Table 4 shows the seasonal mean of energy partitioning at the land surface. In spring, summer, autumn and winter, H/R_n values were 0.46, 0.33, 0.32 and 0.47, and L_E/R_n values were 0.27 0.35, 0.35 and 0.14, respectively. Clearly, H was the main consumer of the net radiation in winter and spring, while L_E was the main consumer of R_n in summer and autumn.

3.4. Soil Temperature and Soil Moisture

[42] Near-surface soil moisture and soil temperature control the apportioning of available energy at the ground surface into sensible and latent heat exchanges with the atmosphere and influence regional climate change further [*Wei*, 1995]. Figure 9 shows the seasonal variations of daily mean soil temperature at depths of 2, 5, 10, 20, 50 and 80 cm, soil moisture at depths of 5, 10, 20, 40 and 80 cm, and 24-h accumulated precipitation at SACOL during the period from January 2007 to December 2008.

[43] Soil temperature in each layer changed seasonally. Although the daily mean of soil temperature showed little difference in shallow layers (2, 5, 10 cm), there were significant differences in deeper layers. The highest soil temperatures occurred during July with values of 303.6, 303.7, 303.4, 301.1, 297.7, and 295.1 K at the depths of 2, 5, 10, 20, 50 and 80 cm, respectively.

[44] Soil moisture is strongly affected by precipitation, especially in shallow layers. Soil moisture in the deep layers had significant differences after heavy rainfall (e.g., in June

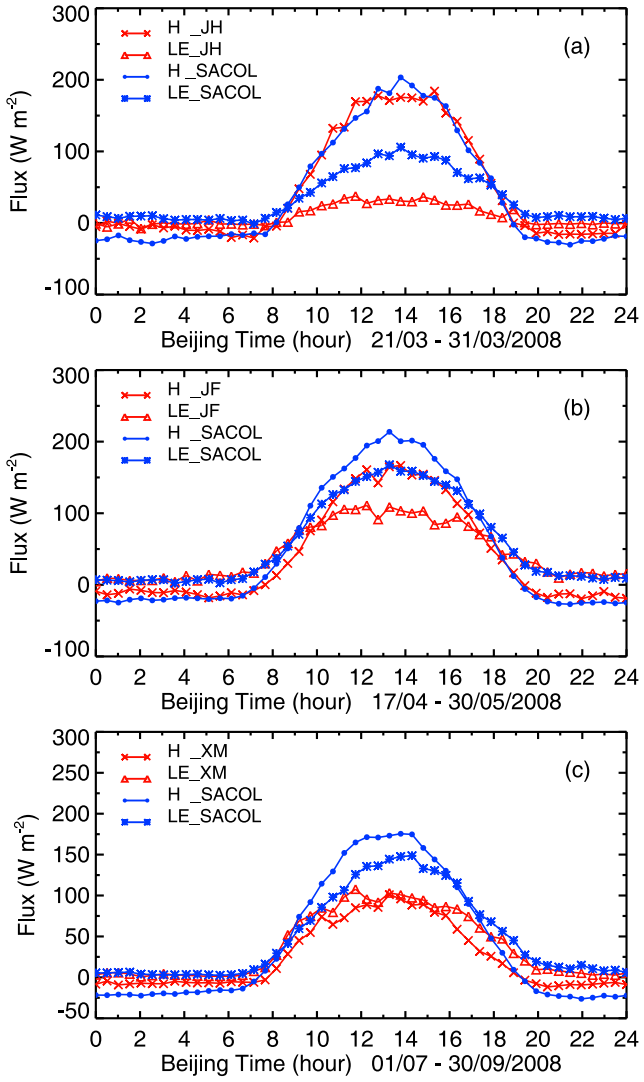

Figure 10. Diurnal variations of sensible heat flux (H) and latent heat flux (L_E) at SACOL, (a) the Jingtai hill site (JH), (b) the Jingtai farmland site (JF), and (c) the Xinglong mountain site (XM) during the experiment periods.

and August 2007). Soil moisture was highest during summer and autumn in 2007. In contrast, soil moisture at 80-cm depth did not change significantly during the wet season of 2008 because few heavy rainfalls occurred in that year. Soil moisture clearly decreased with depth, except the trend between 5-cm depth and 10-cm depth. *Guan et al.* [2009] have analyzed the seasonal variability of soil moisture, surface albedo, and other soil thermal parameters such as heat capacity, thermal conductivity, and thermal diffusivity, and their relationships to soil moisture at SACOL.

3.5. Surface Type Effects

[45] The differences in surface properties and canopy growth at the different land surface types resulted in significant discrepancies in water vapor, heat and energy exchanges [e.g., *Fischer et al.*, 2007; *Li et al.*, 2009]. To better understand the influence to energy partitioning at different types of surfaces in semi-arid areas of the Loess Plateau, flux data collected at the JH, JF, and XM in 2008 were analyzed to explore the spatiotemporal variations of H and L_E and to compare the results with flux data for the same period from SACOL.

[46] Figure 10 plots the diurnal variations of H and L_E at SACOL, JH, JF, and XM during the experimental periods, respectively. Figure 10a shows the diurnal variations of H and L_E at SACOL and JH from 21 to 31 March 2008. L_E at JH was very small and significantly less than that at SACOL, while H was large and approximately equal to that at SACOL. Obviously, the main consumer of R_n at these two sites was H. Figure 10b shows the diurnal variations of H and L_E at SACOL and JF from April 17 to May 31 2008. Both H and L_E have similar diurnal variations at JF and SACOL. But the values of H and L_E at SACOL are generally larger than that at JF. The discrepancy between SACOL and Jingtai could be explained by climate differences between these two sites. Soil moisture content in Jingtai, where is approximately 75 km away from the Tengger Desert, is usually much lower than that at SACOL in the dry season. As land of JF was irrigated by the Yellow River in the spring and summer time, soil moisture at JF is apparently higher than JH, even higher than that at SACOL. Although soil moisture observations both at JH and JF was absent during the experiment time, a confirm conclusion that the discrepancy in soil moisture lead to the differences in energy apportioning still could be established. To some extent, energy apportioning will be influenced by the land-surface type, land cover and land use. Ultimately, soil moisture is the key parameter in controlling energy apportioning. Figure 10c shows the diurnal variation of H and L_E at SACOL and XM from 1 July to 30 September 2008. At these two sites, H was the largest consumer at SACOL, while H and L_E were essentially equal consumers at XM. Although these two sites are only 25 km apart, both H and L_E at SACOL was far greater than XM. It was mainly caused by the different land-surface types present at each site and lead to differences in soil moisture and surface albedo.

[47] Here, analysis was mainly focus on temporal variations in H and L_E over two different land surface types. Figure 11 shows the diurnal variations of monthly mean of H and L_E at SACOL and XM from July to September 2008. At SACOL, H strongly decreased while L_E significantly increased with increasing precipitation during this period. In contrast, there were no such significant changes in H and L_E at XM, although, the total precipitation at XM was larger than SACOL every month. Both H and L_E were approximately equal in July and August, and only in September did L_E become greater than H at XM. H was lager than L_E in July, but become smaller in August and September, with L_E showing the larger increase at SACOL. The results also show that both H and L_E at SACOL was far greater than XM, as it shows in Figure 10. Monthly total precipitation at XM was lager than at SACOL, and H and L_E at SACOL were more sensitive to precipitation, which readily affected the surface soil moisture.

[48] Based on the discussion above, the results demonstrate that H and L_E show significant differences over different land surfaces as a result of differences in vegetation, precipitation and soil moisture. Furthermore, the apportioning of available energy into sensible and latent heat fluxes at the semi-arid area is more sensitive to precipitation and the

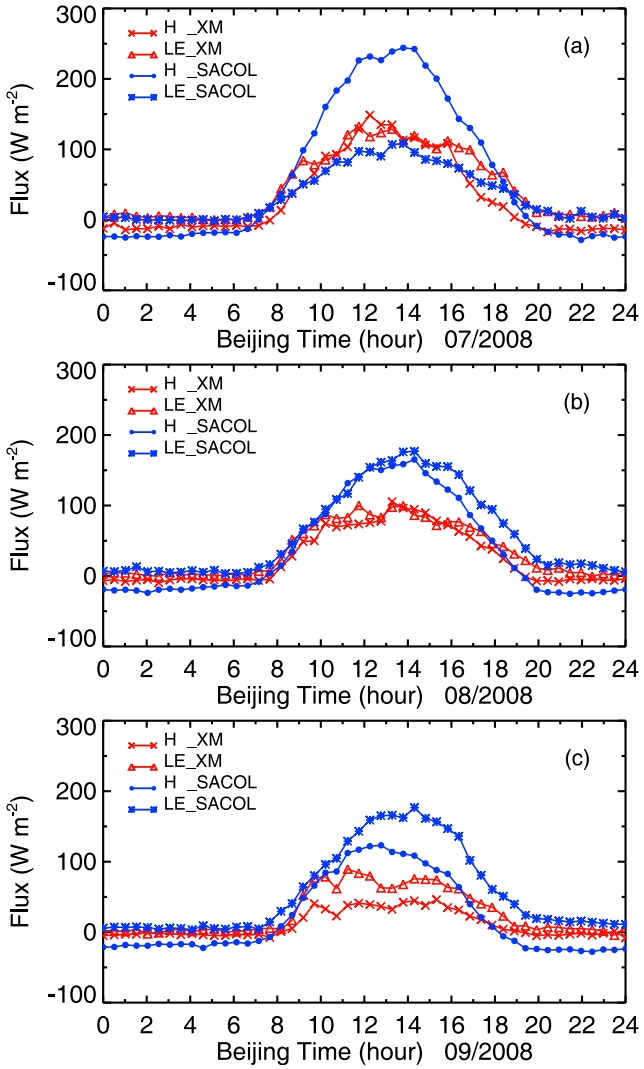

Figure 11. Diurnal variations of sensible heat flux (H) and latent heat flux (L_E) at SACOL and Xinglong mountain site (XM) in (a) July, (b) August, and (c) September 2008.

variation of soil moisture than it at the semi-humid area. Uncertainty water resources provided more uncertainty to the partition of available energy in the semi-arid area.

4. Conclusions

[49] Wind speed, air temperature, water vapor pressure, air pressure, and precipitation measured at SACOL were compared to historical data for the period from January 1956 to December 2008. Our measurement site at SACOL was determined to be representative of the climate for the area.

[50] All four radiative components had distinct seasonal and diurnal cycles, except for the diurnal variation of downward longwave radiation. The highest surface albedo value (0.9) occurred during winter, as result of ground snow cover. Surface albedo was lowest during the wet season due to the high fraction of vegetation cover and wetter soil. Due to the interannual differences in soil moisture, surface albedo showed significant differences between wet and dry years.

[51] Except for the seasonal variation of surface soil heat flux, the energy components changed seasonally and showed dramatic diurnal variations. Sensible (latent) heat flux was the main consumer of available energy in winter and spring (summer and autumn).

[52] Soil moisture is one of the most important factors affecting the portioning of available energy into sensible and latent heat fluxes between the ground surface and the atmosphere. It also influences the surface albedo and the regional climate.

[53] The energy imbalance problem was identified and found that, when the soil heat storage in the surface soil and vegetation canopy was neglected, the energy imbalance ratio was about 22%. While given the surface heat storage calculated by the TDEC method, the imbalance ratio was only 14%. Furthermore, taking the soil heat storage into account, this ratio was reduced to only 8% in spring, and 15% in summer and autumn. Compared with the bare surface layer in spring, it is likely that a part of energy was sorted in the vegetation canopy in summer and autumn.

[54] In addition, we also analyzed the sensible and latent heat fluxes over different land surface types of the Loess Plateau. The results indicate that the sensible and latent heat fluxes exhibited substantial differences over different underlying surfaces due to the differences in vegetation, precipitation, and soil moisture. Furthermore, the apportioning of available energy into sensible and latent heat flux at the semi-arid area is more sensitive to precipitation and the variation of soil moisture than it at the semi-humid area. Uncertainty water resources provided more uncertainty to the partition of available energy at the semi-arid area.

[55] **Acknowledgments.** This study was jointly supported by the National Natural Science Foundation of China under grants 40725015, 40775050, and 40633017 and the National Basic Research Program of China under grant 2006CB400501. We are grateful for the excellent supports provided by the people at SACOL, Lanzhou University, and the history data provided by the China Meteorological Data Sharing Service System. Sincere thanks go to the two anonymous reviewers for their insightful comments and suggestions which further improve the quality of the manuscript.

References

An, Z. S. (2000), The history and variability of the East Asian monsoon, *Quat. Sci. Rev.*, *19*, 171–187, doi:10.1016/S0277-3791(99)00060-8.

An, Z. S., J. E. Kutzbach, W. L. Prell, and S. C. Porter (2001), Evolution of Asian monsoons and phased uplift of the Himalaya-Tibetan plateau since late Miocene times, *Nature*, *411*, 62–66, doi:10.1038/35075035.

Baldocchi, D. D., C. A. Vogel, and B. Hall (1997), Seasonal variation of energy and water vapor exchange rates above and below a boreal jack pine forest canopy, *J. Geophys. Res.*, *102*(D24), 28,939–28,951, doi:10.1029/96JD03325.

Bao, Y., and S. Lu (2006), Review of land-atmosphere interaction research in arid and semi-arid regions (in Chinese), *J. Desert Res.*, *3*, 134–140.

Beljaars, A. C. M., and A. A. M. Holtslag (1991), Flux parameterization over land surfaces for atmospheric models, *J. Appl. Meteorol.*, *30*, 327–341, doi:10.1175/1520-0450(1991)030<0327:FPOLSF>2.0.CO;2.

Bi, X., Z. Gao, X. Deng, D. Wu, J. Liang, H. Zhang, M. Sparrow, J. Du, F. Li, and H. Tan (2007), Seasonal and diurnal variations in moisture, heat, and CO_2 fluxes over grassland in the tropical monsoon region of southern China, *J. Geophys. Res.*, *112*, D10106, doi:10.1029/2006JD007889.

Burba, G. G., S. B. Verma, and J. Kim (1999), Surface energy fluxes of *Phragmites australis* in a prairie wetland, *Agric. For. Meteorol.*, *94*, 31–51, doi:10.1016/S0168-1923(99)00007-6.

Dickinson, R. E. (1995), Land-atmosphere interaction, *U.S. Natl. Rep. Int. Union Geod. Geophys., 1991–1994*, *Rev. Geophys.*, *33*, 917–922.

Dickinson, R. E., A. Henderson-Sellers, C. Rosenzweig, and P. J. Sellers (1991), Evapotranspiration models with canopy resistance for use in

climate models: A review, *Agric. For. Meteorol.*, *54*, 373–388, doi:10.1016/0168-1923(91)90014-H.

Fischer, M. L., D. P. Billesbach, J. A. Berry, W. J. Riley, and M. S. Torn (2007), Spatiotemporal variations in growing season exchanges of CO_2, H_2O, and sensible heat in agricultural fields of the Southern Great Plains, *Earth Interact.*, *11*, 1–21, doi:10.1175/E1231.1.

Foken, T., and S. P. Oncley (1995), Results of the workshop "Instrumental and Methodical Problems of Land Surface Flux Measurements," *Bull. Am. Meteorol. Soc.*, *76*, 1191–1193.

Foken, T., V. P. Kukharets, V. G. Perepelkin, L. R. Tsvang, S. H. Richter, and U. Weisensee (1999), The influence of the variation of the surface temperature on the closure of the surface energy balance, paper presented at 13th Symposium on Boundary Layer and Turbulence, Am. Meteorol. Soc., Dallas, Tex., 10–15 Jan.

Foken, T., M. Göckede, M. Mauder, L. Mahrt, B. Amiro, and W. Munger (2004), Post-field data quality control, in *Handbook of Micrometeorology: A Guide for Surface Flux Measurement and Analysis*, edited by X. Lee et al., pp. 181–208, Kluwer Acad., Dordrecht, Netherlands.

Fu, C. B., and F. Penning De Vries (2006), *Initial Science Plan of the Monsoon Asia Integrated Regional Study*, 86 pp., China Meteorol., Beijing.

Fu, C. B., and G. Wen (2002), Some key issues of aridity trend in northern China (in Chinese), *Clim. Environ. Res.*, *7*, 20–29.

Gao, Z., D. H. Lenschow, Z. He, M. Zhou, L. Wang, Y. Wang, J. He, and J. Shi (2009), Seasonal and diurnal variations in moisture, heat and CO_2 fluxes over a typical steppe prairie in Inner Mongolia, China, *Hydrol. Earth Syst. Sci. Discuss.*, *6*, 1939–1972, doi:10.5194/hessd-6-1939-2009.

Górska, M., J. Vilà-Guerau de Arellano, M. A. LeMone, and C. C. van Heerwaarden (2008), Mean and flux horizontal variability of virtual potential temperature, moisture, and carbon dioxide: Aircraft observations and LES study, *Mon. Weather Rev.*, *136*(11), 4435–4451, doi:10.1175/2008MWR2230.1.

Guan, X., J. Huang, N. Guo, J. Bi, and G. Wang (2009), Variability of soil moisture and its relationship with surface albedo and soil thermal parameters over the Loess Plateau, *Adv. Atmos. Sci.*, *26*(4), 692–700, doi:10.1007/s00376-009-8198-0.

Guo, Z. T., W. F. Ruddiman, Q. Z. Hao, H. B. Wu, Y. S. Qiao, R. X. Zhu, S. Z. Peng, J. J. Wei, B. Y. Yuan, and T. S. Liu (2002), Onset of Asian desertification by 22 Myr ago inferred from loess deposits in China, *Nature*, *416*, 159–163, doi:10.1038/416159a.

Harazono, Y., J. Kim, A. Miyata, T. Choi, J.-I. Yun, and J.-W. Kim (1998), Measurement of energy budget components during the International Rice Experiment (IREX) in Japan, *Hydrol. Processes*, *12*, 2081–2092, doi:10.1002/(SICI)1099-1085(19981030)12:13/14<2081::AID-HYP721>3.0.CO;2-M.

Hu, Y. (1994), Research advance about the energy budget and transportation of water vapor in the HEIFE area (in Chinese), *Adv. Earth Sci.*, *9*, 30–34.

Hu, Y., and Y. Gao (1994), Some new understandings of processes at the land surface in arid area from the HEIFE (in Chinese), *Acta Meteorol. Sin.*, *52*, 285–296.

Huang, J. P., et al. (2008), An overview of the semi-arid climate and environment research observatory over the Loess Plateau, *Adv. Atmos. Sci.*, *25*(6), 906–921, doi:10.1007/s00376-008-0906-7.

Kahan, D. S., Y. Xue, and S. J. Allen (2006), The impact of vegetation and soil parameters in simulations of surface energy and water balance in the semi-arid Sahel: A case study using SEBEX and HAPEX-Sahel data, *J. Hydrol.*, *320*, 238–259, doi:10.1016/j.jhydrol.2005.07.011.

Li, Y. J., L. Zhou, Z. Z. Xu, and G. S. Zhou (2009), Comparison of water vapour, heat and energy exchanges over agricultural and wetland ecosystems, *Hydrol. Processes*, *23*, 2069–2080, doi:10.1002/hyp.7339.

Liu, H., W. Dong, C. Fu, and L. Shi (2004), The long term field experiment on aridification and the ordered human activity in semi-arid area at Tongyu, northeast China (in Chinese), *Clim. Environ. Res.*, *9*, 352–378.

Liu, S., S. G. Li, G. R. Yu, X. M. Sun, L. M. Zhang, Z. M. Hu, Y. N. Li, and X. Z. Zhang (2009), Surface energy exchanges above two grassland ecosystems on the Qinghai-Tibetan Plateau, *Biogeosci. Discuss.*, *6*, 9161–9192, doi:10.5194/bgd-6-9161-2009.

Liu, T. S. (1985), Regional record of aeolian processes: The distribution of loess, in *Loess and the Environment*, 14 pp., China Ocean Press, Beijing.

Lu, D., Z. Chen, J. Chen, G. Wang, J. Ji, H. Chen, Z. Liu, R. Zhang, J. Qiao, and Y. Chen (2002), Composite study on Inner Mongolia semiarid grassland soil-vegetation atmosphere interaction (IMGRASS) (in Chinese), *Earth Sci. Front*, *9*, 52–63.

Lu, D., Z. Chen, J. Chen, G. Wang, J. Ji, H. Chen, and Z. Liu (2005), Study on soil-vegetation-atmosphere interaction in Inner Mongolia semiarid grassland (in Chinese), *Acta Meteorol. Sin.*, *63*, 33–55.

Massman, W. J. (2000), A simple method for estimating frequency response corrections for eddy covariance systems, *Agric. For. Meteorol.*, *104*, 185–198, doi:10.1016/S0168-1923(00)00164-7.

Massman, W. J. (2001), Reply to comment by Rannik on "A simple method for estimating frequency response corrections for eddy covariance systems," *Agric. For. Meteorol.*, *107*, 247–251, doi:10.1016/S0168-1923(00)00237-9.

Moore, C. J. (1986), Frequency response corrections for eddy correlation systems, *Boundary Layer Meteorol.*, *37*, 17–35, doi:10.1007/BF00122754.

Panin, G. N., G. Tetzlaff, A. Raabe, H. J. Schönfeld, and A. E. Nasonov (1996), Inhomogeneity of the land surface and the parametrization of surface fluxes: A discussion, *Wiss. Mitt. Inst. Meteorol. Univ. Inst. Troposphärenforsch. Leipzig*, *4*, 204–215.

Rosset, M., M. Riedo, A. Grub, M. Geissmann, and J. Fuhrer (1997), Seasonal variation in radiation and energy balances of permanent pastures at different altitudes, *Agric. For. Meteorol.*, *86*, 245–258, doi:10.1016/S0168-1923(96)02423-9.

Rowntree, P. R. (1991), Atmospheric parameterization schemes for evaporation over land: Basic concepts and climate modeling aspects, in *Land Surface Evaporation: Measurement and Parameterization*, edited by T. J. Schmugge and J.-C. André, pp. 5–29, Springer, New York.

Schotanus, P., F. T. M. Nieuwstadt, and H. A. R. De Bruin (1983), Temperature measurement with a sonic anemometer and its application to heat and moisture fluctuations, *Boundary Layer Meteorol.*, *26*, 81–93, doi:10.1007/BF00164332.

Toda, M., K. Nishida, N. Ohte, M. Tani, and K. Musiake (2002), Observations of energy fluxes and evapotranspiration over terrestrial complex land covers in the tropical monsoon environment, *J. Meteorol. Soc. Jpn.*, *80*, 465–484, doi:10.2151/jmsj.80.465.

Wang, J. M., and Y. Mitsuta (1991), Turbulence structure and transfer characteristics in the surface layer of the HEIFE Gobi area, *J. Meteorol. Soc. Jpn.*, *69*, 587–593.

Wang, J. M., and Y. Mitsuta (1992), Evaporation from the desert: Some preliminary results of HEIFE, *Boundary Layer Meteorol.*, *59*, 413–418, doi:10.1007/BF02215461.

Wang, K., P. Wang, J. Liu, M. Sparrow, S. Haginoya, and X. Zhou (2005), Variation of surface albedo and soil thermal parameters with soil moisture content at a semi-desert site on the western Tibetan Plateau, *Boundary Layer Meteorol.*, *116*, 117–129, doi:10.1007/s10546-004-7403-z.

Webb, E. K., G. I. Pearman, and R. Leuning (1980), Correction of flux measurements for density effects due to heat and water vapour transfer, *Q. J. R. Meteorol. Soc.*, *106*, 85–100, doi:10.1002/qj.49710644707.

Wei, M. Y. (1995), *Soil Moisture: Report of a Workshop Held in Tiburon, California*, *NASA Conf. Publ.*, *3319*, 80 pp.

Wicke, W., and C. Bernhofer (1996), Energy balance comparison of the Hartheim forest and an adjacent grassland site during the HartX experiment, *Theor. Appl. Climatol.*, *53*, 49–58, doi:10.1007/BF00866410.

Wilczak, J. M., S. P. Oncley, and S. A. Stage (2001), Sonic anemometer tilt correction algorithms, *Boundary Layer Meteorol.*, *99*, 127–150, doi:10.1023/A:1018966204465.

Wohlfahrt, G., A. Hammerle, A. Haslwanter, M. Bahn, U. Tappeiner, and A. Cernusca (2008), Seasonal and inter-annual variability of the net ecosystem CO_2 exchange of a temperate mountain grassland: Effects of weather and management, *J. Geophys. Res.*, *113*, D08110, doi:10.1029/2007JD009286.

Yang, K., and J. Wang (2008), A temperature prediction-correction method for estimating surface soil heat flux from soil temperature and moisture data, *Sci. China, Ser. D*, *51*(5), 721–729.

Yi, C., K. J. Davis, P. S. Bakwin, B. W. Berger, and L. C. Marr (2000), Influence of advection on measurements of the net ecosystem-atmosphere exchange of CO_2 from a very tall tower, *J. Geophys. Res.*, *105*(D8), 9991–9999, doi:10.1029/2000JD900080.

Zhang, H. S., J. Y. Chen, and S. U. Park (2001), Turbulence structure in the unstable condition over various surfaces, *Boundary Layer Meteorol.*, *100*, 243–261, doi:10.1023/A:1019223316895.

Zhang, L. M., and Z. P. Shangguan (2002), Relationship between the soil moisture and the vegetation productivity in the Loess Plateau (in Chinese), *Arid Zone Res.*, *19*(4), 59–63.

Zhang, Q., X. Cao, G. Wei, and H. Ronghui (2002), Observations and study of land surface parameters over Gobi in typical arid region, *Adv. Atmos. Sci.*, *19*(1), 121–135, doi:10.1007/s00376-002-0039-3.

Zhang, Q., et al. (2005), NWC-ALIEX and its advances (in Chinese), *Adv. Earth Sci.*, *20*, 60–74.

Zhou, J. L., X. H. Hou, and G. L. Ji (1992), Preliminary study of solar radiation properties in HEIFE area in late summer (in Chinese), *Plateau Meteorol.*, *11*(4), 381–388.

Zuo, J. Q., et al. (2009), Surface turbulent flux measurements over the Loess Plateau for a semi-arid climate change study, *Adv. Atmos. Sci.*, *26*(4), 679–691, doi:10.1007/s00376-009-8188-2.

J. Bi, J. Huang, Z. Huang, J. Shi, G. Wang, and J. Zuo, Key Laboratory for Semi-Arid Climate Change of the Ministry of Education, College of Atmospheric Sciences, Lanzhou University, Lanzhou, 730000, China. (hjp@lzu.edu.cn)

W. Guo, ICGCR, School of Atmospheric Sciences, Nanjing University, Nanjing, 210093, China.

J. Wang, Cold and Arid Regions Environmental and Engineering Research Institute, Chinese Academy of Sciences, Lanzhou 73000, China.